nature immunology

Opposing macrophage polarization programs show extensive epigenomic and transcriptional cross-talk

Viviana Piccolo[1,6], Alessia Curina[1,6], Marco Genua[2], Serena Ghisletti[3], Marta Simonatto[3], Arianna Sabò[4], Bruno Amati[1,4], Renato Ostuni[2,7] & Gioacchino Natoli[1,5,7]

Stimulation of macrophages with interferon-γ (IFN-γ) and interleukin 4 (IL-4) triggers distinct and opposing activation programs. During mixed infections or cancer, macrophages are often exposed to both cytokines, but how these two programs influence each other remains unclear. We found that IFN-γ and IL-4 mutually inhibited the epigenomic and transcriptional changes induced by each cytokine alone. Computational and functional analyses revealed the genomic bases for gene-specific cross-repression. For instance, while binding motifs for the transcription factors STAT1 and IRF1 were associated with robust and IL-4-resistant responses to IFN-γ, their coexistence with binding sites for auxiliary transcription factors such as AP-1 generated vulnerability to IL-4-mediated inhibition. These data provide a core mechanistic framework for the integration of signals that control macrophage activation in complex environmental conditions.

When exposed to micro-environmental stimuli, macrophages acquire new functional properties in a dynamic and reversible fashion[1]. The M1 program and M2 program, instigated by exposure to interferon-γ (IFN-γ) and interleukin 4 (IL-4), respectively, represent two extreme poles of a broad spectrum of macrophage-activation states[2] and were named after the cytokines specifically produced by lymphocytes of the T_H1 and T_H2 subsets of helper T cells[3,4]. While the M1 program is typically associated with a pro-inflammatory phenotype and high microbicidal activity, M2 macrophages are linked to resistance to helminths and tissue repair[5,6]. Although characterization of these two functional extremes has contributed greatly to advancement of the understanding of macrophage biology, several elements of complexity must be taken into consideration. First, macrophage-activation states are in principle as diverse as the variety of stimuli these cells can be exposed to[2]. Second, such activation states, although associated with some forms of cellular memory[7–9], do not drive terminal and irreversible differentiation programs, which indicates the possibility of inter-conversion between macrophage states when micro-environmental conditions change[10]. Third, macrophages are exposed to multiple and often conflicting micro-environmental stimuli that might affect their biology in a complex fashion[11].

The co-existence of antagonistic signals that affect macrophage function is frequently observed *in vivo*. Upon co-infection with pathogens that elicit type 1 immunity and type 2 immunity (such as viruses and helminths, respectively), the pathways that lead to the release of IFN-γ and IL-4 are concomitantly activated, and the interaction between these conflicting programs has important biological consequences. The activation of an IL-4-dependent type 2 immune response to helminths results in a broad spectrum of immunoregulatory and immunosuppressive effects[12,13] that also depend on myeloid cells[14,15]. In keeping with those findings, epidemiological data indicate that helminths interfere with the ability of the immune system to control co-infection by microbial pathogens[16] and that macrophages activated by IL-4 favor *Mycobacterium tuberculosis* replication[17,18]. Similar events are observed in conditions in which a single pathogen, such as *Leishmania major*, concomitantly triggers M1 responses and M2 responses[19]. Furthermore, both in tumors and during the resolution phase of inflammation, macrophages are co-exposed to pro-inflammatory signals and anti-inflammatory signals that drive concomitant and frequently co-existing M1 and M2 profiles[20]. Collectively, these observations highlight the need to delineate the relationships between multiple environmental signals to understand their effect on macrophage biology.

Here we set out to address some critical and basic aspects of macrophage polarization: whether the M1- and M2-polarization programs are mutually exclusive; whether one of the two programs is dominant over the other; and, finally, the mechanisms underlying the cross-talk between M1-polarizing stimuli and M2-polarizing stimuli. Transcriptional and epigenomic profiling of macrophages treated with IL-4 or IFN-γ or a combination of these showed that each cytokine exerted inhibitory effects on the opposite activation program. These effects were of broad amplitude but in most cases of limited magnitude, indicative of a lack of mutual exclusivity of the M1 and M2 programs and a high degree of macrophage plasticity. However, the

[1]Department of Experimental Oncology, European Institute of Oncology, Milan, Italy. [2]San Raffaele Telethon Institute for Gene Therapy, Division of Regenerative Medicine, Stem Cells and Gene Therapy, IRCCS San Raffaele Scientific Institute, Milan, Italy. [3]Humanitas Clinical and Research Center, Milan, Italy. [4]Center for Genomic Science of IIT@SEMM, Fondazione Istituto Italiano di Tecnologia, Milan, Italy. [5]Department of Biomedical Sciences, School of Medicine, Humanitas University, Milan, Italy. [6]These authors contributed equally to this work. [7]These authors jointly directed this work. Correspondence should be addressed to G.N. (gioacchino.natoli@hunimed.eu) or R.O. (ostuni.renato@hsr.it).

Received 19 July 2016; accepted 14 February 2017; published online 13 March 2017; doi:10.1038/ni.3710

induction of selected genes encoding products with critical biological roles, as well as hundreds of enhancers characteristic of either program, was strongly suppressed upon co-stimulation. While binding of the transcription factors STAT1 and IRF1 was associated with the resistance of IFN-γ-responsive enhancers to IL-4-mediated inhibition, the involvement of auxiliary transcription factors, such as AP-1 and C/EBPβ, generated vulnerability to the inhibitory effects of IL-4. In the context of IL-4-dependent macrophage activation, induction of the transcription factor Myc was instead needed to trigger a component of the response that was resistant to IFN-γ-mediated inhibition. These data provide a mechanistic framework for the interpretation of cross-regulatory effects of stimuli that drive opposing macrophage-activation programs.

RESULTS

Cross-regulation of macrophage-polarization programs

We used a high-throughput RNA-based sequencing approach (RNA-seq) in mouse bone-marrow-derived macrophages (BMDMs) to determine the effects of the co-stimulation with IL-4 and IFN-γ on the gene-expression programs induced by cytokines administered individually. In pilot studies, we determined the optimal stimulus concentrations: the minimal dose required for IL-4 and IFN-γ to stimulate phosphorylation of the transcription factors STAT6 and STAT1, respectively, and for maximal induction of canonical M2 genes and M1 genes such as *Arg1* and *Nos2*, respectively (**Supplementary Fig. 1a**). Flow cytometry and immunofluorescence analysis (**Supplementary Fig. 2**) with antibodies that recognize the phosphorylated forms of the transcription factors STAT1 (phosphorylated at Tyr701) and STAT6 (phosphorylated at Tyr641) showed that these critical mediators of the IFN-γ-induced program and the IL-4-induced program, respectively, were activated within the same cells in the analyzed population. BMDMs were stimulated for 2 h or 4 h and poly-adenylated RNA was extracted and sequenced at high depth (biological triplicates; **Supplementary Table 1**). The overall correlation among samples was very high (R^2 range, 0.974–0.990) (**Supplementary Fig. 1b**). We first analyzed the effects of the co-stimulation on the genes induced at 2 h or 4 h by IFN-γ (454 or 827, respectively) or IL-4 (209 or 332, respectively). For both IFN-γ-induced genes and IL-4-induced genes, co-administration of the other cytokine caused transcriptional cross-inhibition of the respective program that was both broad in amplitude and overall limited in magnitude, at both 2 h (**Fig. 1a**) and 4 h (**Fig. 1b**) after stimulation. Downregulation of IFN-γ-induced genes by co-stimulation with IL-4 became more evident at 4 h (**Fig. 1b**), which suggested that genes induced by IFN-γ with slower kinetics were more sensitive to inhibition by IL-4. A relatively small fraction of the IFN-γ- and IL-4-induced genes were especially sensitive to co-stimulation and showed almost complete inhibition by the antagonistic stimulus (**Fig. 1b** and **Supplementary Table 2**). Notably, genes encoding canonical markers of M1 or M2 polarization were included in this category. For example, induction of *Nos2* (which encodes inducible nitric-oxide synthase) and *Ccl5* (which encodes the chemokine CCL5) were strongly inhibited by IL-4 at the level of mRNA (**Fig. 1c**) and protein (**Supplementary Fig. 1c**). Similarly, the M2-signature genes *Arg1* (which encodes arginase 1) and *Retnla* (which encodes the adipokine Relm-α) were induced by IL-4 and repressed by co-stimulation with IFN-γ (**Fig. 1c**, **Supplementary Fig. 1d** and **Supplementary Table 2**). The transcriptional antagonism between IFN-γ and IL-4 at the genes analyzed persisted over longer times of co-stimulation (**Fig. 1d**) and occurred through a broad range of concentrations, being in some cases influenced by the dose of cytokine (**Supplementary Fig. 1d**). Moreover, consistent with the increased susceptibility to co-stimulation of genes induced late by IFN-γ, transcription of *Nos2* and *Ccl5* by IFN-γ, which peaked at over 4 h after stimulation, was inhibited by the addition of IL-4 even after stimulation with IFN-γ (**Supplementary Fig. 1e**). In some cases, as for *Ccl24*, co-stimulation increased gene expression above the levels obtained with individual stimuli (**Fig. 1a**,**b**), but this occurrence was uncommon. Finally, IL-4-mediated inhibition of IFN-γ-induced gene expression was abolished in *Stat6*$^{-/-}$ BMDMs (**Supplementary Fig. 3**), which suggested it required STAT6. Overall, these data indicated that IFN-γ and IL-4 exerted mutual transcriptional antagonism in BMDMs.

Lack of mutual antagonism at the signaling level pathways

We next investigated the mechanistic bases of the interaction between IFN-γ and IL-4 in BMDMs. IFN-γ-induced phosphorylation of STAT1 and of the kinases ERK1/2 and AKT was unaffected by co- or pre-administration of IL-4, and induction of STAT6 phosphorylation occurred normally in the presence of IFN-γ (**Supplementary Fig. 4a**). Moreover, conditioned supernatants of IL-4-treated BMDMs, in which IL-4 was inactivated with a neutralizing antibody, were unable to inhibit the IFN-γ-stimulated induction of *Nos2* and *Ccl5* (**Supplementary Fig. 4b**); this indicated that the inhibitory effects of the co-stimulation were not mediated by the autocrine activities of soluble molecules released into the culture medium. Because macrophages might be exposed to different cytokines in sequential or temporally distinct waves *in vivo*, we determined whether the inhibition mediated by IL-4 persisted after its removal from the cell-culture medium. BMDMs were conditioned with IL-4 for 4 h, then were washed and stimulated with IFN-γ 24 h after the addition of fresh medium. In all cases assessed, transient pre-conditioning with IL-4 reduced the expression of IFN-γ-induced genes (**Supplementary Fig. 4c**), which indicated a short-term memory effect of the conditioning of macrophages by IL-4. Collectively, these data indicated a cell-intrinsic regulatory mechanism that controlled the IL-4–IFN-γ cross-talk downstream of cytokine-induced signaling pathways.

Mutual repression of cytokine-induced histone acetylation

Because individual genes showed differential sensitivity to the inhibitory effects of the co-stimulation, we investigated whether the *cis*-regulatory elements (enhancers and promoters) controlling the transcription of co-stimulation-sensitive genes had a composition and organization different from that of those controlling co-stimulation-resistant genes. We used chromatin immunoprecipitation coupled to next-generation sequencing (ChIP-seq) to map genome-wide changes in histone acetylation (H3K27ac) in BMDMs stimulated for 2 and 4 h with IFN-γ or IL-4 or a combination of these. Histone acetylation is associated with active *cis*-regulatory elements[21,22] and is dynamically regulated in response to acute stimulation[7,23], reflective of changes in the binding or activity of sequence-specific transcription factors. We focused on the inducible histone-acetylation events at 2 h and 4 h that were selectively activated by either IFN-γ or IL-4 (**Fig. 2a** and **Supplementary Table 3**). The following main trends were evident. First, co-administration of IFN-γ and IL-4 caused a global decrease in inducible H3K27ac triggered by either IFN-γ or IL-4 alone (**Fig. 2b**). Second, the repressive effects of IFN-γ on the IL-4 program were of greater magnitude than those exerted by IL-4 on the IFN-γ program, particularly at 2 h (**Fig. 2c**), which suggested a dominance of IFN-γ over IL-4. Third, IFN-γ and IL-4 seemed to repress the deposition of H3K27ac by the antagonistic stimulus in a temporally different manner (**Fig. 2b**,**c**). While repression of IL-4-induced histone acetylation by IFN-γ was already maximal at 2 h after stimulation, IL-4-dependent

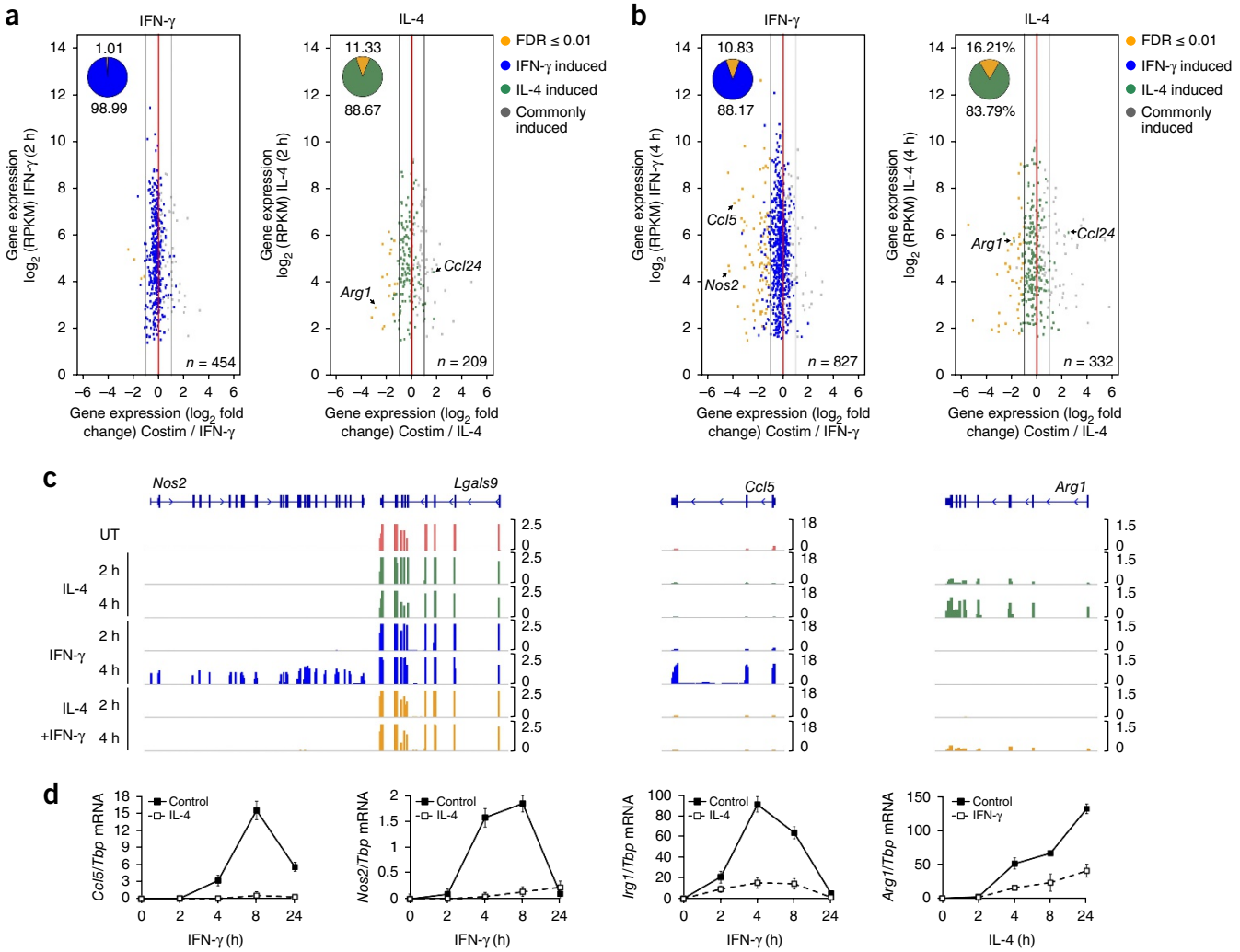

Figure 1 Effects of co-stimulation on the transcriptional programs induced by IFN-γ and IL-4. (**a**,**b**) Vertical axes: expression of genes (log_2 of the RPKM, reads per kilobase per million mapped reads) after stimulation for 2 h (**a**) or 4 h (**b**) with IFN-γ (left) or IL-4 (right). Horizontal axes: log_2 of the fold change in gene expression after costimulation relative to stimulation with IFN-γ alone (left) or IL-4 alone (right). Blue and green dots (key) indicate genes selectively induced by IFN-γ or IL-4, respectively, identified on the basis of a false-discovery rate (FDR) of ≤0.01 and a change in expression of twofold or more relative to expression in the untreated condition. Orange dots indicate genes whose inhibition by co-stimulation was significant (FDR ≤ 0.01; key) and higher than twofold (log_2 fold change ≥ ±1) relative to expression after stimulation with IFN-γ or IL-4 alone. *n* = number of genes. Inset, frequency of genes in each category. (**c**) RNA-seq snapshots of *Nos2*, *Lgals9* (which encodes the lectin Gal-9), *Ccl5* and *Arg1* after stimulation for 2 or 4 h with IFN-γ or IL-4 or both. Numbers on the right indicate reads per million (RPM). (**d**) RT-qPCR analysis of *Ccl5*, *Nos2*, *Irg1* and *Arg1* after stimulation for various times (horizontal axes) with IFN-γ (left three plots) or IL-4 (far right), in control conditions or in the presence of the opposing cytokine (key). mRNA levels are presented relative to those of the control gene *Tbp*. Data are from three independent experiments.

repression of IFN-γ responses was detectable at 4 h only (**Fig. 2b**,**c**), which suggested the involvement of transcription factors that acted late in the response, such as those whose expression was induced by IFN-γ. As representative examples, the histone acetylation of several enhancers upstream of *Nos2* was induced by IFN-γ and suppressed by co-stimulation with IL-4, while the histone acetylation induced by IFN-γ in the *Gbp3* locus was not substantially affected by IL-4 (**Fig. 2d** and **Supplementary Table 3**).

The transcription-factor-binding sites associated with regions showing inducible histone acetylation in response to IFN-γ partially differed at 2 h and 4 h (**Fig. 2e** and **Supplementary Table 4**). At 2 h, the most over-represented binding motif was the canonical STAT1-binding site GAS ('γ-activated sequence'), which enables direct binding of STAT1 homodimers, followed by an IRF motif to which STAT1 is recruited via complexes with an IRF protein that provides DNA-binding specificity[24] (**Fig. 2e**). At 4 h, the most over-represented transcription-factor-binding sites in regions acetylated in response to IFN-γ were variants of canonical IRF-binding sites, while STAT1 motifs were not retrieved anymore (**Fig. 2e**). To determine the molecular bases of those findings, we generated ChIP-Seq data sets for STAT1 in BMDMs that were either left untreated or stimulated for 2 h and 4 h with IFN-γ. Consistent with the motif-discovery analysis, binding of STAT1 was increased genome wide at 2 h after stimulation and returned to baseline at 4 h, along with a reduction in the abundance of phosphorylated STAT1 (**Supplementary Fig. 5a–c**). At the genomic regions at which H3K27ac was induced by stimulation with IL-4, a canonical STAT6-binding site was the most over-represented motif at both time points (**Fig. 2f**).

To obtain additional insight into the cross-regulation between IFN-γ and IL-4, we analyzed the genomic distribution of STAT1

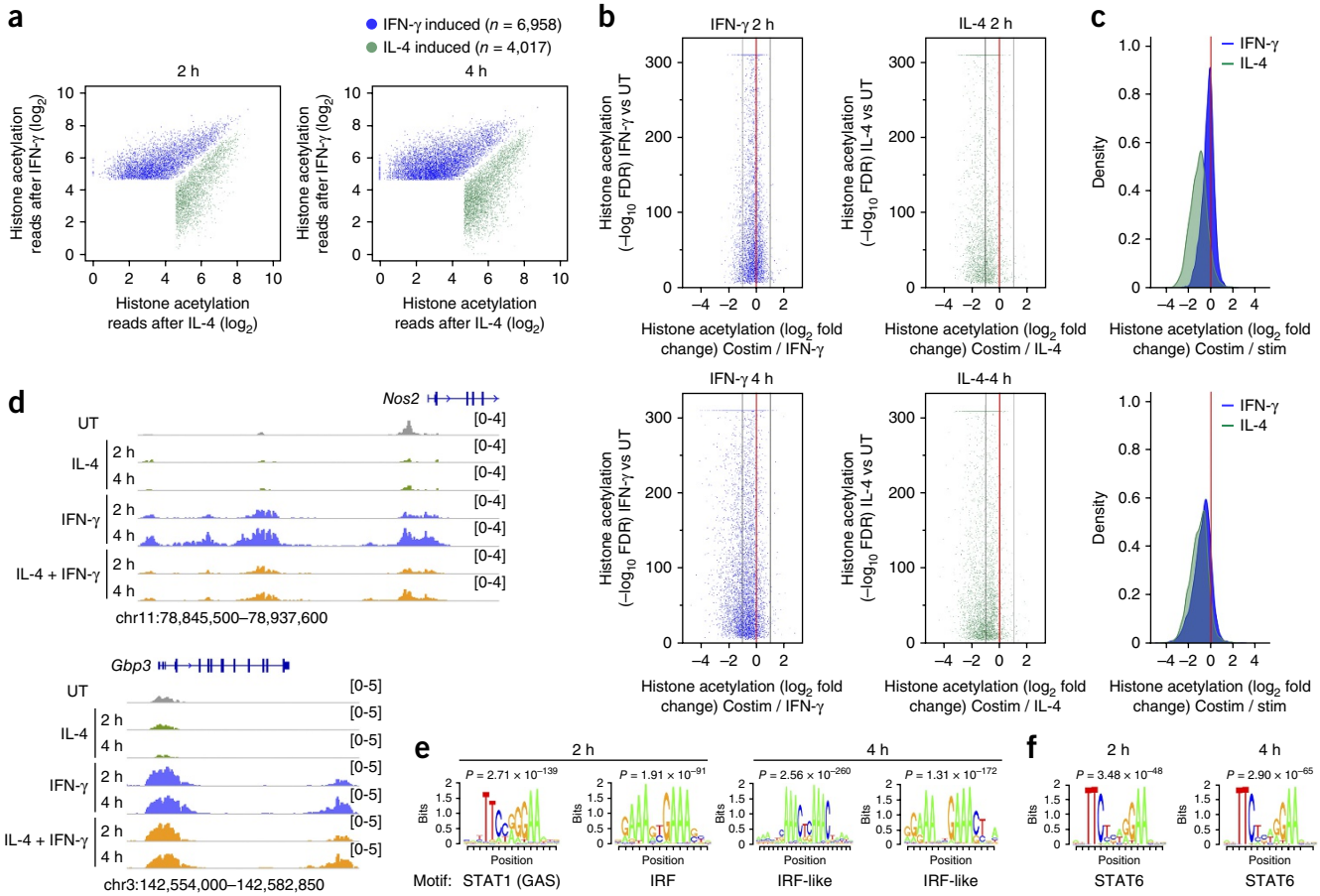

Figure 2 Cross-regulation of histone acetylation induced by IFN-γ and IL-4. (**a**) H3K27ac histone acetylation events induced in cells stimulated for 2 h (left) or 4 h (right) with IFN-γ or IL-4 (key). (**b**) Histone acetylation in BMDMs stimulated for 2 h (top) or 4 h (bottom) with IFN-γ (left; blue) or IL-4 (right; green) in the absence or in the presence of the opposing cytokine. Vertical axes: FDR ($-\log_{10}$ values) obtained by comparison of histone acetylated regions in stimulated cells versus unstimulated (UT) cells. Horizontal axes: $\log_2$ values of fold changes in acetylation in co-stimulated cells relative to cells stimulated with IFN-γ or IL-4 alone. (**c**) Histone acetylation changes induced by co-stimulation in BMDMs stimulated for 2 h (top) or 4 h (bottom) with IFN-γ or IL-4 (key). Vertical axes: relative acetylation density. Horizontal axes: $\log_2$ values of fold changes in acetylation in co-stimulated cells relative to that in cells stimulated with IFN-γ or IL-4 alone. (**d**) ChIP-Seq snapshots showing histone acetylation (H3K27ac) at the *Nos2* locus (top) and *Gpb3* locus (bottom) in cells left untreated (UT) or stimulated for 2 h or 4 h with IL-4, IFN-γ or both. Numbers on the right margin indicate reads per million. (**e**,**f**) Over-representation analysis of consensus transcription factor binding motifs within regulatory elements induced by stimulation for 2 h or 4 h (above plots) with IFN-γ (**e**) or IL-4 (**f**). Data are representative of two independent experiments.

and STAT6 in BMDMs. 14,576 STAT1 peaks were detected 2 h after stimulation with IFN-γ (**Fig. 3a**), and co-stimulation with IL-4 had a marginal impact on this (**Fig. 3b** and **Supplementary Table 5**), which indicated that the antagonistic effect of IL-4 on IFN-γ-induced histone acetylation could not be ascribed to diminished association of STAT1 with its genomic targets. Consistent with that, STAT1-binding events and STAT6-binding events were similarly frequent in the proximity of IL-4-resistant genes and IL-4-sensitive genes, and they were unaffected by co-stimulation (**Fig. 3a**). 23,306 STAT6 peaks were detected above the threshold in IL-4-stimulated BMDMs (**Fig. 3a**). Co-treatment with IFN-γ caused a trend toward a reduction in the association of STAT6 with chromatin, although IL-4-induced binding was maintained, in general (**Fig. 3c**,**d**). As examples of this, the decrease in IFN-γ-induced histone acetylation caused by costimulation with IL-4 at the *Ccl5* and the *Rsad2-Cmpk2* locus (which encodes viperin and the kinase TDK1) was not associated with detectable changes in occupancy by STAT1 (**Fig. 3e**). The *Arg1* locus showed slight but detectable attenuation in the recruitment of STAT6 upon co-stimulation with IFN-γ (**Fig. 3e**). The DNA sequences that were significantly over-represented in the STAT1 peaks included both GAS motifs and IRF-binding motifs (data not shown), which suggested that the recruitment of STAT1 occurred via both direct DNA binding and IRF-mediated DNA binding; however, the DNA sequences associated with STAT6 peaks included canonical STAT6-binding motifs and IRF- and/or PU.1-like motifs (data not shown). Overall, these data indicated that at the level of both the transcriptome and the epigenome, co-stimulation induced a continuum of inhibitory effects over the changes caused by IFN-γ or IL-4 administered individually.

DNA-sequence features of inducibly acetylated genomic regions

To delineate the genomic bases of the different sensitivity of *cis*-regulatory elements to the inhibitory effects of the opposing cytokine, we defined discrete sub-groups of enhancers with clearly different responses to co-stimulation and compared those with each other. We first focused on IFN-γ-activated elements. At one extreme, we identified 773 genomic regions whose histone acetylation was induced by IFN-γ

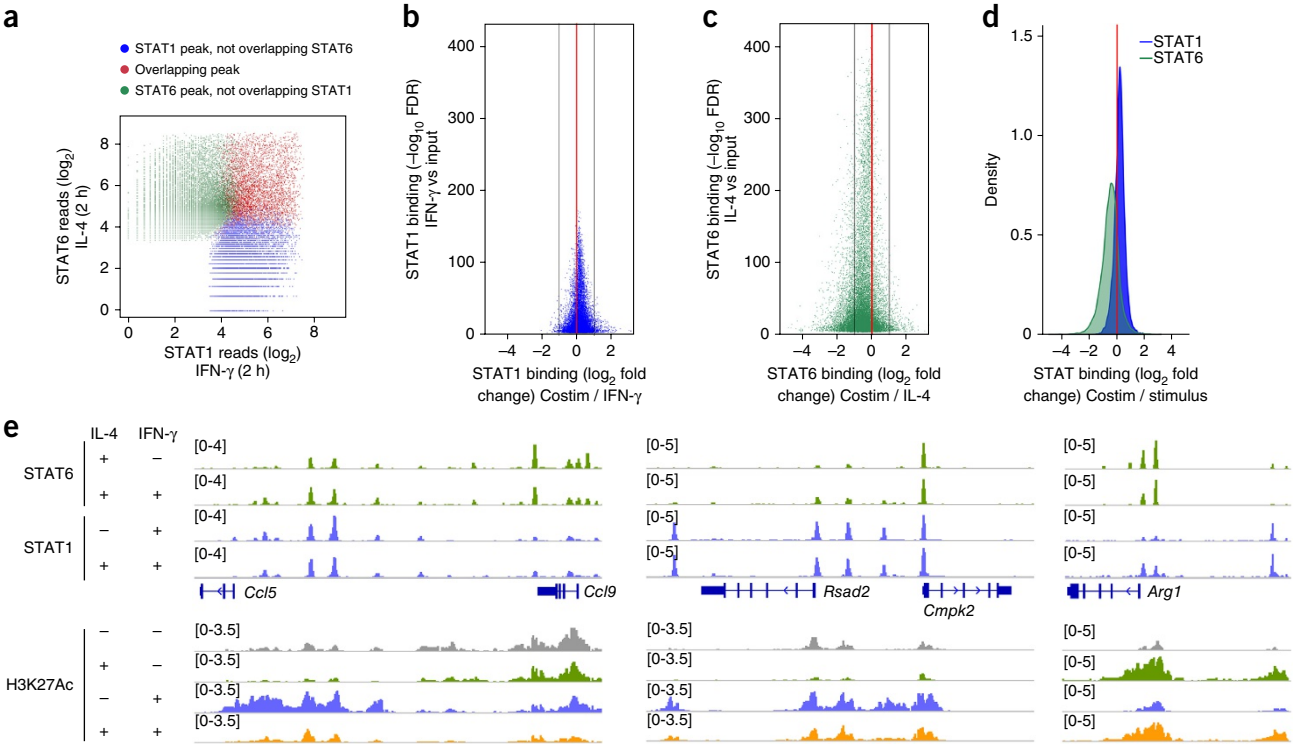

Figure 3 Binding of STAT1 and STAT6 in response to stimulation with IFN-γ or IL-4 or both. (**a**) STAT6 peaks induced by 2 h of stimulation with IL-4, plotted against STAT1 peaks induced by 2 h of stimulation with IFN-γ, showing overlapping and non-overlapping peaks (key). (**b**,**c**) Binding of STAT1 (**b**) in cells stimulated for 2 h with IFN-γ in the absence or presence of IL-4 and binding of STAT6 (**c**) in cells stimulated with IL-4 in the absence or presence of IFN-γ. Results are presented as FDR ($-\log_{10}$ values) for stimulated cells versus input (vertical axis) plotted against $\log_2$ values of the fold change in binding in co-stimulated cells relative to that in cells stimulated with IFN-γ or IL-4 alone (horizontal axis). (**d**) Genomic binding of STAT1 or STAT6 (key) in co-stimulated cells relative to cells stimulated with IFN-γ or IL-4 alone. Data are presented as relative binding density of STAT1 or STAT6 (vertical axis) plotted against $\log_2$ values of the fold change in STAT1 or STAT6 binding in co-stimulated cells relative to that in cells stimulated with IFN-γ or IL-4 alone. (**e**) Binding of STAT6 or STAT1 (top) and H3K27ac signals (bottom) at cross-regulated genomic loci in cells treated with various combinations of IL-4 and IFN-γ; results are presented as reads per million. Data are representative of two independent experiments.

and was highly sensitive to the inhibitory effects of co-stimulation (**Fig. 4a**,**b**). At the other end, we identified 736 IFN-γ-inducible *cis*-regulatory elements that were completely resistant to co-stimulation (**Fig. 4a**,**b** and **Supplementary Table 6**). We next used motif-enrichment analysis to identify significantly over-represented transcription-factor-binding motifs in the group of IL-4-sensitive enhancers and the group of IL-4 resistant enhancers. Both the IL-4-sensitive subset and the IL-4-resistant subset of IFN-γ-inducible enhancers showed similarly significant over-representation of STAT- and IRF-binding motifs relative to the abundance of such motifs in the FANTOM5 collection of active enhancers[25] (**Fig. 4c** and **Supplementary Table 7**). Therefore, the molecular bases for the responsiveness of both classes of elements to IFN-γ stimulation seemed to be similar and seemed to be linked to the activation of STAT1–IRF1 (ref. 24). However, in a direct comparison of IL-4-sensitive enhancers versus IL-4-resistant enhancers, we noted over-representation of binding sites for the transcription factors AP-1, ATF, C/EBP and NF-κB in the IL-4-sensitive group (**Fig. 4c** and **Supplementary Table 8**). IL-4-resistant elements did not show any highly significant enrichment for transcription-factor binding motifs relative to the abundance of such motifs in the IL-4-sensitive elements (**Fig. 4c** and **Supplementary Table 8**). Overall, the main difference between IL-4-resistant elements activated by IFN-γ and their IL-4-sensitive counterparts seemed to be the presence, in the IL-4-sensitive group, of motifs recognized by transcription factors other than STAT1 and IRF1.

Transcription factors that mediate the inhibitory effects of IL-4

The data reported above led us to investigate whether a genomic response mediated exclusively by STAT1 and IRF1 might by default be resistant to the inhibitory effects of IL-4 and, conversely, whether the dependence of a *cis*-regulatory element on additional transcription factors other than STAT1–IRF1 (such as members of the AP-1 and C/EBP families) determined its vulnerability to IL-4. First, we analyzed in BMDMs the genomic distribution of IRF1, whose mRNA was induced by IFN-γ in a sustained and IL-4-resistant manner (**Fig. 4d** and **Supplementary Fig. 4a**) and found that, similar to STAT1, it was largely unaffected by co-stimulation with IL-4 (**Supplementary Fig. 6**). We next analyzed the expression or activity, in BMDMs stimulated with IFN-γ without or with IL-4, of auxiliary transcription factors whose consensus DNA-binding sites were over-represented in IL-4-sensitive enhancers. Among those, *Cebpb* (which encodes C/EBPβ) and *Junb* (which encodes the transcription factor JUNB) were induced by IFN-γ and were repressed by co-stimulation with IL-4 (**Fig. 4d** and **Supplementary Table 7**). Moreover, the *Junb* and *Cebpb* loci were bound by both STAT1 and STAT6 in response to co-stimulation (**Fig. 4e**), suggestive of direct cross-regulation.

Those observations prompted us to determine the roles of C/EBPβ and JUNB as mediators of the transcriptional program induced by IFN-γ and of its cross-talk with IL-4. We used ChIP-Seq to analyze the genomic distribution of C/EBPβ and JUNB in BMDMs stimulated

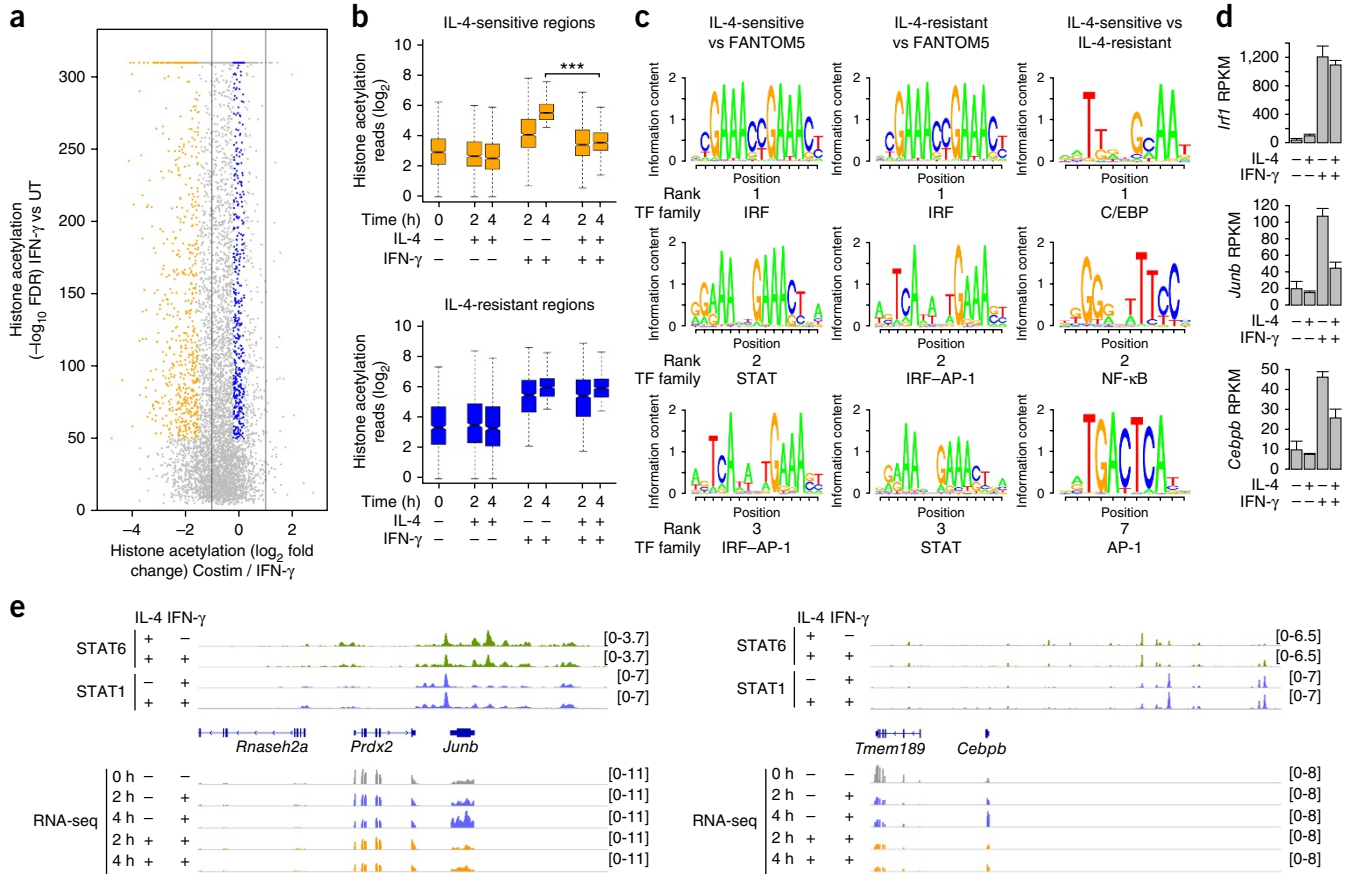

Figure 4 Characterization of IL-4-sensitive and IL-4-resistant groups of enhancers induced by IFN-γ. (**a**) Genomic regions showing increased histone acetylation after 4 h treatment with IFN-γ were divided into an IL-4-sensitive group (orange dots) and an IL-4-resistant group (blue dots). All other regions with IFN-γ-inducible H3K27ac are shown as grey dots. Vertical axis: FDR ($-\log_{10}$ values) obtained by SICER comparison of stimulated cells versus unstimulated cells (UT). Horizontal axis: $\log_2$ values of fold changes in acetylation in co-stimulated cells relative to that of cells stimulated with IFN-γ alone. (**b**) Quantification of histone-acetylation levels in the IL-4-sensitive and IL-4-resistant regions (as in **a**) in cells treated for 0, 2 or 4 h with various combinations (below plots) of IL-4 and IFN-γ. $***P = 3.53 \times 10^{-128}$. (**c**) Over-representation analysis of transcription-factor motifs within IL-4-sensitive and IL-4-resistant regions, relative to their abundance in the FANTOM5 collection of active enhancers (left and middle) or in a cross-comparison (right) (complete analyses and ranks based on statistical values, **Supplementary Tables 7** and **8**). (**d**) RNA-seq analysis of selected transcription factors belonging to the IRF (top), AP-1 (middle) and C/EBP (bottom) families. (**e**) Binding of STAT6 and STAT1 (2 h IFN-γ) to (top) and RNA-seq analysis (bottom) of *JunB* and *Cebpb* and adjacent genes (presented for comparison) in cells stimulated with various combinations of IL-4 and IFN-γ; results are presented as reads per million. Data are representative of two independent experiments in all panels except **d** (three replicates; mean + s.e.m.).

for 4 h with IFN-γ in the presence or absence of IL-4 and found that the binding of both transcription factors to DNA was significantly lower in co-stimulated BMDMs than in those stimulated with IFN-γ alone (**Fig. 5a**,**b**). We next analyzed the IFN-γ-induced histone acetylation and gene expression of BMDMs depleted of *Junb* or *Cebpb* through lentivirus-mediated delivery of interfering short hairpin RNA (shRNA) (**Supplementary Fig. 7**). We sorted the IFN-γ-inducible JUNB and C/EBPβ ChIP-seq peaks into discrete subgroups—those most inhibited by IL-4 and those least affected by IL-4 (**Fig. 5a–d**)—then analyzed the effects of depletion of *Junb* or *Cebpb* on the abundance of H3K27ac in response to IFN-γ at the two groups of regions. Knockdown of *Junb* resulted in a significant, albeit moderate reduction in the abundance of H3K27ac at genomic regions at which the binding of JUNB was strongly inhibited by IL-4 but not at those regions at which the binding of JUNB was resistant to IL-4 (**Fig. 5c**), which indicated that binding of JUNB contributed to the deposition of H3K27ac in response to IFN-γ and that its depletion was a partial phenocopy of the inhibition by co-stimulation with IL-4. In contrast, knockdown of *Cebpb* had no clear effect on IFN-γ-induced histone acetylation at sites of IL-4-sensitive or IL-4-resistant occupancy by C/EBPβ (**Fig. 5d**). JUNB peaks and, to a lesser extent, C/EBPβ peaks were more commonly found in the proximity of IL-4-sensitive genes than in the proximity of their IL-4-resistant counterparts (**Fig. 5e**,**f** and **Supplementary Table 9**). Notably, depletion of *Junb* and *Cebpb* 'preferentially' impaired the activation of IFN-γ-inducible genes that were sensitive to inhibition by IL-4 (**Fig. 5e**,**f** and **Supplementary Table 10**). As an example, *Nfkbiz* (which encodes a regulator of the NF-κB family of transcription factors) and *Cd69* (which encodes the C-type lectin CD69) were dependent on JUNB for their inducibility by IFN-γ, while *Acsl1* (which encodes an isozyme of the long-chain fatty-acid-coenzyme A ligase family) and *Il27* (which encodes the cytokine IL-27) were dependent on CEBPβ and, to a lesser extent, on JUNB (**Fig. 5g**). Together these data indicated that IFN-γ-inducible genes whose activation required auxiliary transcription factors (such as JUNB and C/EBPβ) in addition to STAT1 and IRFs were vulnerable to the inhibitory effects of IL-4.

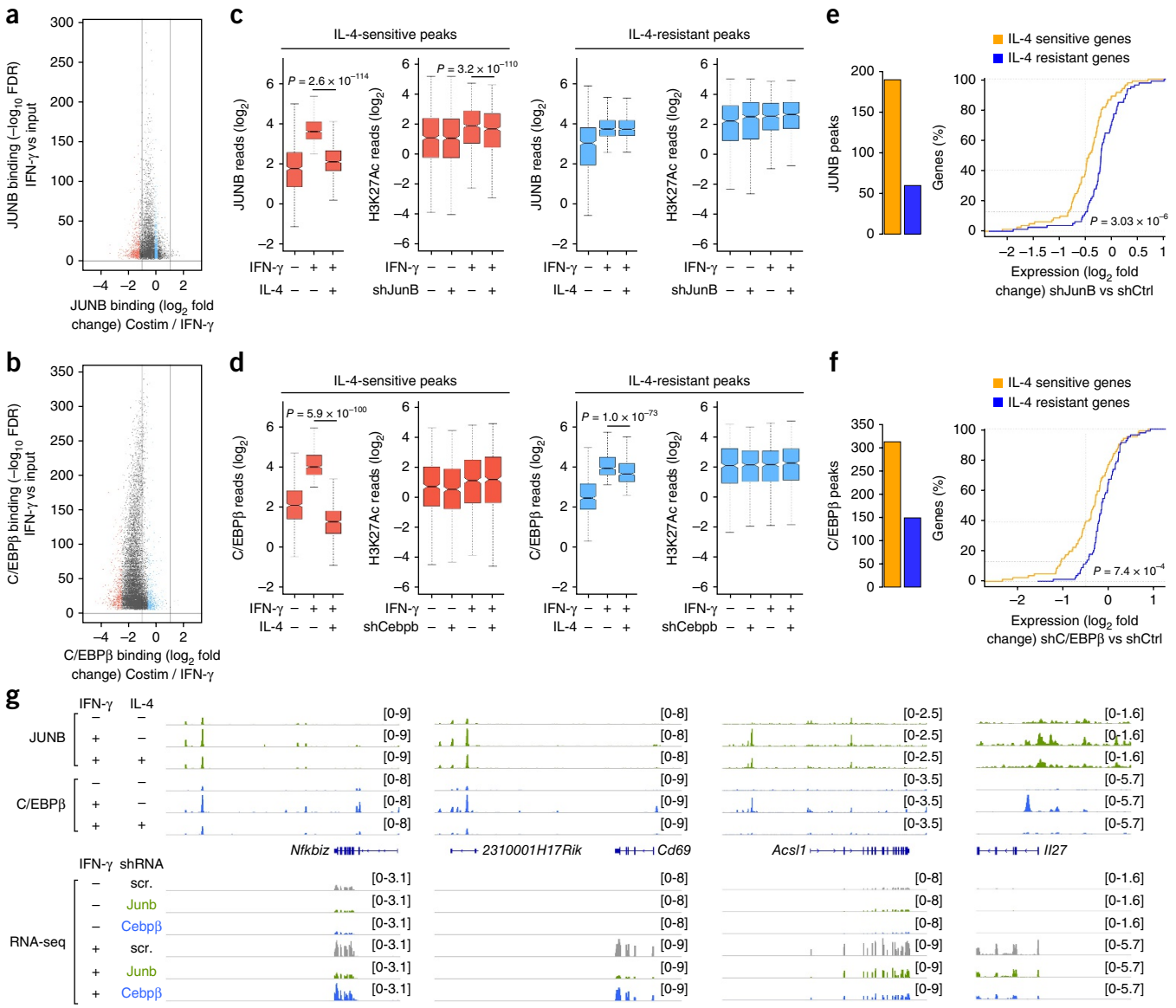

Figure 5 Analysis of the roles of JUNB and C/EBPβ in the IFN-γ response and IL-4-mediated antagonism. (**a**,**b**) ChIP-seq analysis of JUNB (**a**) and C/EBPβ (**b**) in macrophages stimulated for 4 h with IFN-γ in the presence or absence of IL-4. Data are shown as FDR ($-\log_{10}$ values) for IFN-γ-treated cells versus untreated cells (vertical axes) plotted against $\log_2$ values of the fold change in transcription factor binding in co-stimulated cells relative to that in cells stimulated with IFN-γ alone (horizontal axes). Regions highly sensitive (red) or relatively resistant (light blue) to inhibition by IL-4 are indicated. All other regions are indicated as black dots. (**c**,**d**) Binding of JUNB (**c**) or C/EBPβ (**d**) in cells treated with the indicated combinations of IFN-γ and IL-4, shown separately at IL-4-sensitive and IL-4-resistant regions. Histone acetylation (**c**,**d**) is shown at the same regions in untreated or IFN-γ-treated cells transduced with JUNB-specific shRNA (+) (**b**) or C/EBPβ-specific shRNA (+) (**d**) or control shRNA with scrambled sequence (–). (**e**,**f**) JUNB peaks (**e**) and C/EBPβ peaks (**f**) in proximity to IFN-γ-inducible genes that were sensitive or resistant (key) to IL-4-mediated inhibition (left). Right: frequency (presented as empiric cumulative distribution functions) of IL-4-sensitive genes and IL-4-resistant genes (key) with various changes in expression (horizontal axes) in cells transduced with JUNB-specific shRNA (**e**) or C/EBPβ-specific shRNA (**f**) relative to their expression in cells transduced with control shRNA. (**g**) ChIP-seq snapshots of the binding of JUNB and C/EBPβ to *Nfkbiz, Cd69, Acsl1* and *Il27* in cells stimulated with various combinations of IL-4 and IFN-γ. Bottom panels show RNA-seq data of the same genes in untreated or IFN-γ-treated cells transduced with JUNB-specific or C/EBPβ-specific shRNA or control shRNA. Results are presented as reads per million. Data are representative of two independent experiments.

Genomic roles of Myc in the IL-4–IFN-γ interaction

We next analyzed over-represented transcription-factor-binding motifs in the sets of IL-4-activated *cis*-regulatory regions whose histone acetylation was most or least sensitive to IFN-γ-mediated inhibition (**Fig. 6a**,**b**). Because of the strong inhibitory effect of IFN-γ on the genomic response induced by IL-4, we were able to analyze only a small set of 317 acetylated regions resistant to cross-inhibition by IFN-γ. The IFN-γ-sensitive group showed considerable enrichment for the STAT6-binding motif relative to the abundance of this motif in the FANTOM5 collection of active enhancers (**Fig. 6c** and **Supplementary Table 11**), consistent with the genome-wide attenuation of STAT6 binding in BMDMs co-stimulated with IFN-γ. In a direct comparison, the IFN-γ-sensitive enhancers showed enrichment for consensus DNA-binding sites for the transcription factor MAF

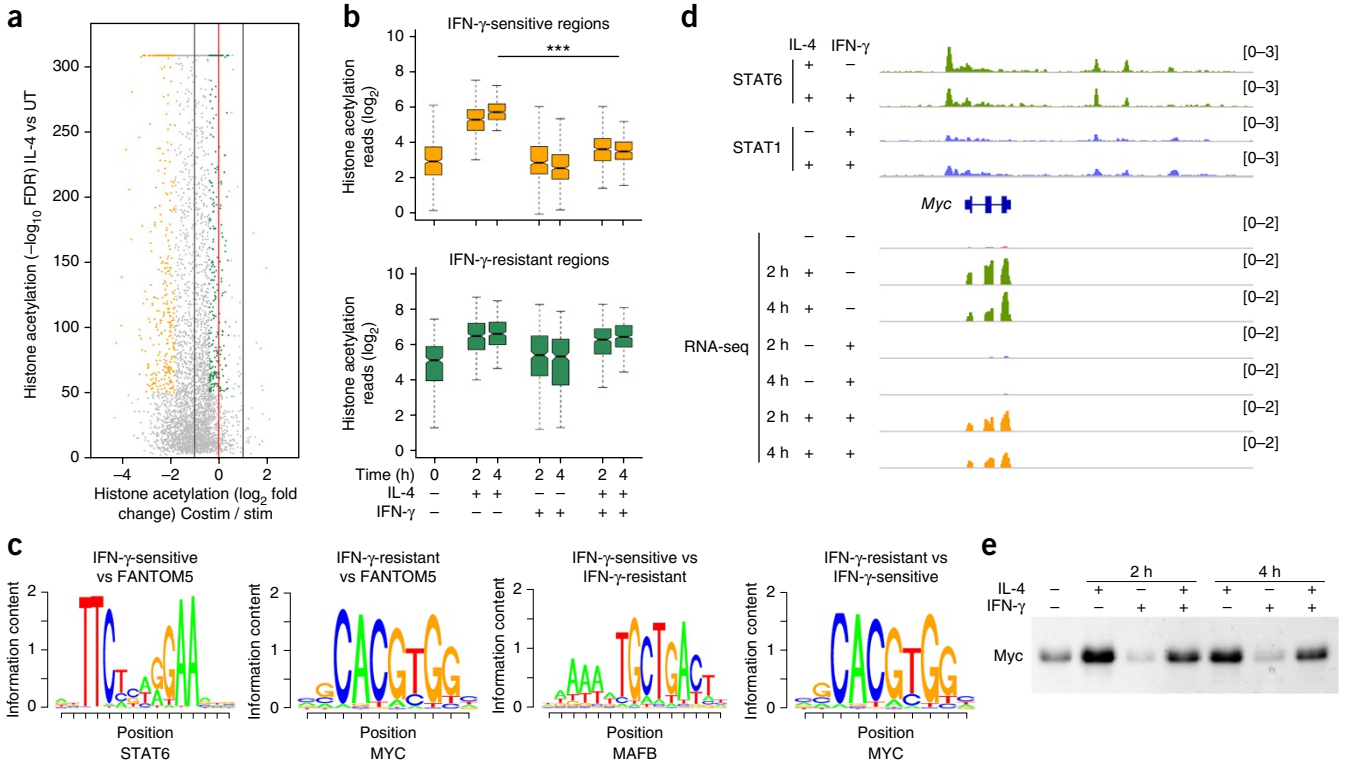

Figure 6 Analysis of the *cis*-regulatory bases for inhibition of IL-4-mediated macrophage activation by IFN-γ. (**a**) Genomic regions showing increased histone acetylation after 4 h treatment with IL-4 were divided into an IFN-γ-sensitive group (orange dots) and an IFN-γ-resistant group (green dots). All other regions with IL-4-inducible H3K27ac are shown as grey dots. Data are presented as FDR ($-\log_{10}$ values) obtained by SICER comparison of IL-4-stimulated cells versus unstimulated cells (UT) (vertical axis) plotted against $\log_2$ values of fold changes in acetylation in co-stimulated cells relative to that in cells stimulated with IL-4 alone (horizontal axis). (**b**) Quantification of histone-acetylation levels in the IFN-γ-sensitive and IFN-γ-resistant groups (as in **a**) in cells treated for 0, 2 or 4 h with the indicated combinations of IL-4 and IFN-γ. $***P = 2.004 \times 10^{-60}$. (**c**) Over-representation of transcription-factor motifs in the IFN-γ-sensitive and IFN-γ-resistant regions (as in **a**), relative to their abundance in the FANTOM5 collection (left) or in a cross-comparison (right); below plot, top-ranked motif (based on *P*-value) in each comparison (complete analysis, **Supplementary Table 11**). (**d**) Snapshot showing binding of STAT6 and STAT1 to the *Myc* locus in cells treated for 2 h with the indicated combinations of IL-4 and IFN-γ. Bottom: RNA-seq data in cells treated for 2 or 4 h with IL-4 with or without IFN-γ; data are presented as Reads Per Million. (**e**) Immunoblot analysis of Myc in BMDMs treated for 2 h or 4 h with the indicated combinations of IL-4 and IFN-γ. Data are representative of two independent experiments.

relative to the abundance of such motifs in the set of IFN-γ-resistant regulatory elements (**Fig. 6c**); this might have been related to the inhibitory effect of IFN-γ on IL-4-mediated induction of *MafB* (which encodes the transcription factor MAFB) (**Supplementary Table 2**). Conversely, the motif for which the IFN-γ-resistant enhancers showed the greatest enrichment (relative to its abundance in the FANTOM5 collection) was the canonical E-box recognized by Myc (**Fig. 6c**), which is transcriptionally induced by IL-4 (ref. 26). The STAT6-binding site was also over-represented in this subset of genomic regions, but its enrichment was less significant than that of Myc (**Supplementary Table 11**). Consistent with that, E-boxes were also over-represented in IFN-γ-resistant elements relative to their abundance in IFN-γ-sensitive elements, together with motifs with an abundance of guanosine-cytosine, which relates to the high frequency of E-boxes in CpG dinucleotide islands (**Fig. 6c** and **Supplementary Table 12**). The expression of Myc mRNA and protein was induced by IL-4 (**Fig. 6d**,**e**), probably via direct binding of STAT6 to the *Myc* promoter (**Fig. 6d**), and this response was largely preserved in BMDMs co-stimulated with IFN-γ (**Fig. 6d**,**e**). These data suggested that Myc, a transcription factor associated mainly with the control of proliferation, might participate in the IL-4 response downstream of STAT6 and that the Myc-dependent genomic regulation of IL-4-activated enhancers might confer robustness to antagonistic signals.

To directly address those possibilities, we analyzed the genomic distribution of Myc in BMDMs left untreated or treated for 2 h or 4 h with IL-4. While Myc bound to a limited number of sites (433 peaks over background) in unstimulated BMDMs, it generated 11,357 peaks at 2 h and 8,747 peaks at 4 h after stimulation (**Fig. 7a** and **Supplementary Table 13**). The intensity of Myc's binding decreased over time (**Fig. 7b**), along with a slight decrease in the level of protein (**Fig. 6e**). Myc bound in the vicinity of not only genes encoding products associated with housekeeping functions, such as mRNA metabolism and the cell cycle, but also genes encoding products linked to immune-system-related gene-ontology terms, such as 'immune response' and 'interferon signaling' (**Fig. 7c**). Clustering analysis showed that Myc-bound regions could be separated into a small cluster associated with substantial recruitment of STAT6, abundant H3K27ac, the STAT6 motif and the E-box motif (cluster 1; 11.6% of peaks) and two larger groups with limited or negligible binding of STAT6, high acetylation (cluster 2) or low acetylation (cluster 3), and a strong over-representation of the E-box motif (clusters 2 and 3) (**Fig. 7d** and **Supplementary Table 14**). Cluster 1 showed selective enrichment for gene-ontology terms associated with immune responses, while clusters 2 and 3 both showed enrichment for canonical Myc-associated gene-ontology terms, such as 'RNA metabolism' and 'cell cycle' (**Fig. 7d** and **Supplementary Table 15**). BMDMs co-stimulated with IL-4 and

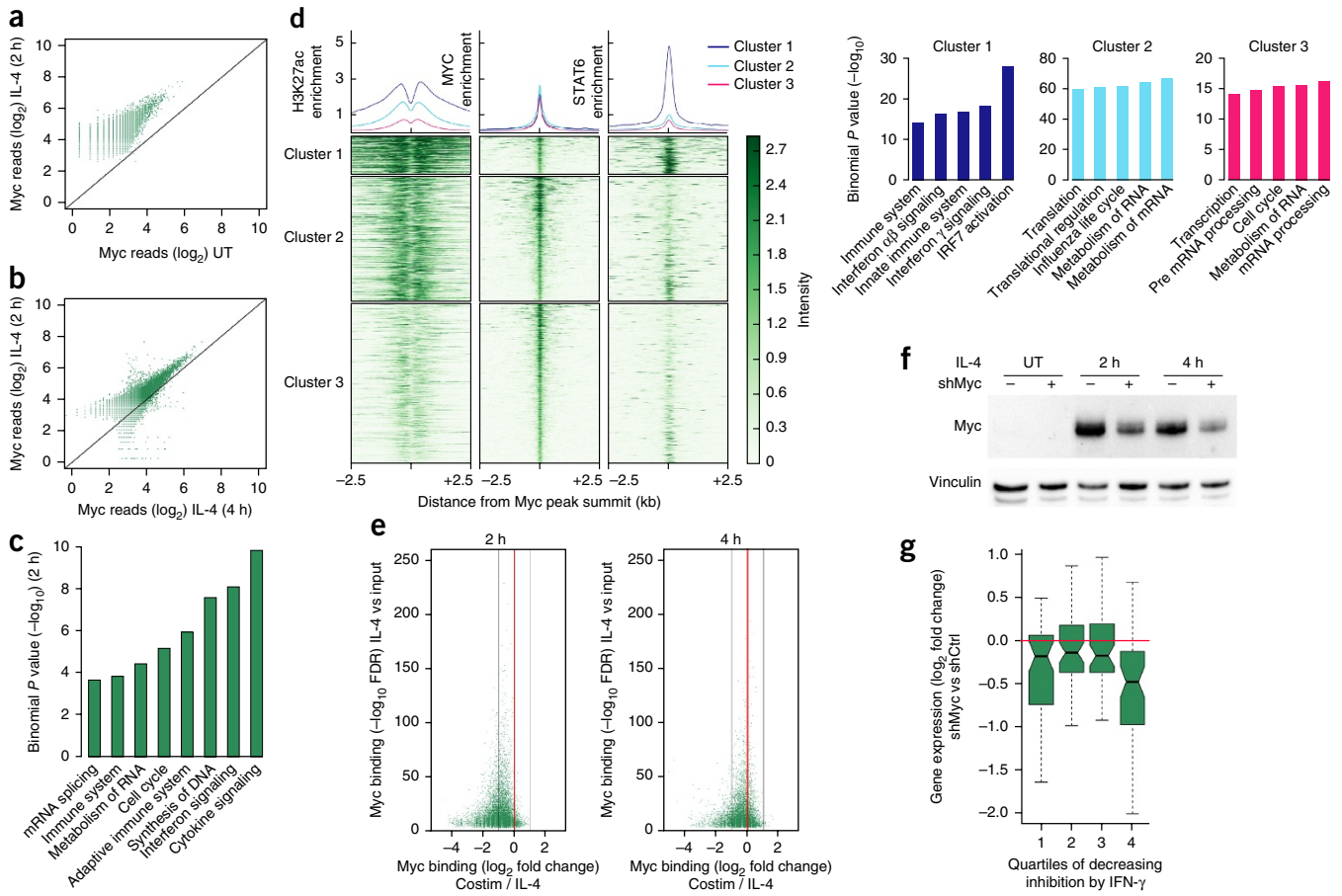

Figure 7 Involvement of Myc in the IL-4-dependent response. (**a**,**b**) Myc occupancy in the genome of untreated BMDMs versus BMDMs treated for 2 h with IL-4 (**a**); or in BMDMs treated for 2 h with IL-4 versus BMDMs treated for 4 h with IL-4 (**b**). (**c**) Selected gene-ontology categories retrieved from GREAT (genomic regions enrichment of annotations tool) of ChIP-seq data for Myc in cells treated for 2 h with IL-4. (**d**) ChIP-seq analysis of H3K27ac (left), Myc (middle) and STAT6 (right) in cells treated for 2 h with IL-4. Average read coverage over clusters is shown. All signals are centered on the summit of Myc peaks and extended for ± 2.5 kilobases (kb). Gene-ontology categories associated with each cluster (retrieved by GREAT) are on the right. (**e**) Genomic occupancy of Myc in BMDMs treated for 2 h (left) and 4 h (right) with IL-4 with or without co-treatment with IFN-γ Data are presented as FDR ($-\log_{10}$ values) for IL-4-treated cells versus untreated cells left plotted against $\log_2$ values of the fold change in binding in co-stimulated cells relative to that in cells stimulated with IL-4 alone. (**f**) Immunoblot analysis of Myc and vinculin (loading control) in cells transduced with Myc-specific shRNA (shMyc +) or control shRNA (shMyc –) and treated for 0, 2 or 4 h (above blots) with IL-4. (**g**) Expression of IL-4-inducible genes in cells transduced with Myc-specific shRNA (shMyc) relative to their expression in cells transduced with control shRNA (shCtrl) and treated for 2 h with IL-4. IL-4 inducible genes were categorized into quartiles by the inhibitory effect of IFN-γ co-stimulation: strongest (first quartile) to weakest (fourth quartile) (horizontal axis). Data are representative of two independent experiments.

IFN-γ showed less genomic occupancy by Myc than that of IL-4-stimulated BMDMs (**Fig. 7e**), consistent with the partial reduction in the level of its mRNA and protein upon co-stimulation.

To directly address the role of Myc in the IL-4 response, we depleted BMDMs of Myc via lentivirus-mediated delivery of shRNA (**Fig. 7f**). We then used RNA-seq to analyze the response of BMDMs depleted of Myc to IL-4 at 2 h and 4 h, compared with that of BMDMs treated with control shRNA. We assigned the IL-4-induced genes to four quartiles on the basis of their sensitivity to the inhibitory effects of IFN-γ (determined in the experiments described above); the first quartile included the genes inhibited most by IFN-γ, and the fourth quartile included the genes inhibited least by IFN-γ. Although knockdown of Myc showed broad effects of low magnitude, it had a greater effect in the IL-4-induced genes most resistant to IFN-γ (**Fig. 7g**). Overall, depletion of Myc reduced the expression of 54 IL-4-inducible genes, which included mainly IFN-γ-resistant genes, such as *Ch25h*, *Cd274*, *Ccl2*, *Ccl7*, *Ccl12*, *Flt1* and *Serpina3f* (**Supplementary Table 16**).

DISCUSSION

In this study, we identified key principles that govern the interaction between stimuli that drive macrophage function toward contrasting programs. This framework may provide the basis for a more systematic mechanistic analysis of the interaction among macrophage activators in physiology and disease.

The IL-4- and IFN-γ-driven polarization states entailed distinct and non-overlapping gene-expression changes that reflected the dynamic evolution of the transcriptional regulatory circuits activated by polarizing cytokines. In co-stimulated cells, IFN-γ and IL-4 were still able to induce their specific gene-expression programs and the associated epigenomic changes. However, co-stimulation with IL-4 and IFN-γ extensively, yet only partially, attenuated the responses elicited by each stimulus alone. Overall, the IFN-γ- and the IL-4-induced programs were able to co-exist to a large extent, but in conditions of co-stimulation with IL-4 and IFN-γ, macrophages were 'stretched' between two opposite functional poles, which resulted in the reciprocal attenuation of both. In a sense, co-delivery of the two polarizing cytokines showed

the remarkable extent and, at the same time, the maxima to which macrophage plasticity can be driven.

Neither the transcriptional effects nor the epigenomic effects of co-stimulation were homogeneous; instead, they were more evident at subsets of genes and *cis*-regulatory elements. Specifically, the induction of a small number of M1 signature genes or M2 signature genes, such as *Nos2* and *Arg1*, respectively, was almost completely abolished in the presence of the antagonistic cytokine, while the induction of many others, such as typical interferon-stimulated genes encoding antiviral products, was unaffected. Robustness of the IFN-γ-elicited program is essential for preventing an extreme increase in susceptibility to infections when type 2 immunity is concomitantly activated. At the same time, the inhibitory activity of IL-4 on the IFN-γ-activated program and the suppression of some genes encoding products involved in microbial killing, such as *Nos2*, might explain the negative effect of type 2 immunity on resistance to some infections.

Although the cross-inhibition between IL-4 and IFN-γ probably entails multiple regulatory circuits, we identified some basic mechanistic principles. Simple *cis*-regulatory elements containing only the minimal motifs responsive to IFN-γ (GAS and IRF sites) were resistant to the antagonistic effects of IL-4. Conversely, susceptibility to inhibition by IL-4 was limited to complex *cis*-regulatory elements containing, in addition to GAS and IRF sites, motifs for auxiliary transcription factors such as JUNB, whose expression was induced by IFN-γ and antagonized by co-stimulation with IL-4. Such different genomic organization of *cis*-regulatory elements that control IFN-γ-activated genes reflects an optimal solution to two opposing needs that become evident when macrophages are exposed to multiple stimuli: maintaining the robustness of IFN-γ-stimulated responses critical for survival to infections while at the same time enabling the plasticity needed to modulate macrophage properties in response to complex inputs[12].

The antagonistic regulation of IL-4-induced gene-expression and chromatin changes by IFN-γ followed different rules, as the binding of STAT6 to cognate sites was globally attenuated by IFN-γ. While that finding is consistent with an overall dominance of the IFN-γ-induced program over the IL-4-induced program, the mechanisms underlying this effect are still unclear. Our data also demonstrated involvement of Myc, a hub in the control of cell proliferation[27], in the IFN-γ-resistant component of the IL-4 response. Myc was induced by IL-4, was bound to a set of genomic regions largely distinct from those occupied by STAT6 and contributed to the activation of a large panel of IL-4-inducible genes. Because IL-4 is required for macrophage proliferation during parasitic infections[28,29], it is likely that Myc contributes to this response. However, the requirement for Myc in the IL-4-induced activation of genes encoding many immune-response molecules, such as chemokines of the CCL family, hints at a broader role for Myc in the IL-4 response.

An additional aspect is the possibility that STAT1 and STAT6 might exert a direct mutual control on each other's activity at a large number of genomic regulatory elements. In response to IFN-γ, STAT1 also bound many regulatory elements associated with IL-4-inducible genes. Analogously, IL-4-activated STAT6 bound a sizeable fraction of the regulatory elements of IFN-γ-activated genes. Overall, a large fraction of STAT1- and STAT6-binding events occurred at overlapping or nearby genomic regions. These data hint at a genomic organization that enables mutual inhibitory interactions between STAT1 and STAT6. Whether different combinations of signals with pro- and anti-inflammatory functions produce similar outcomes will require additional investigation. In this context, IFN-γ and lipopolysaccharide have been shown to act synergistically to enhance the induction of cytokine production in macrophages through a process dependent on chromatin priming[30].

The interplay between IFN-γ and IL-4 has important biological implications, since these cytokines frequently coexist *in vivo*. The cross-talk between these cytokines might be involved in the transition from pro-inflammatory programs to anti-inflammatory programs during resolution of inflammation; it might underlie some of the pathogenic effects observed during co-infections with pathogens that elicit type 1 or type 2 immune responses; and it might explain complex and diverging phenotypes of macrophages associated with different tumors.

METHODS

Methods, including statements of data availability and any associated accession codes and references, are available in the online version of the paper.

Note: Any Supplementary Information and Source Data files are available in the online version of the paper.

ACKNOWLEDGMENTS

We thank Silvia Monticelli for critical feedback on the manuscript; L. Rotta, T. Capra and S. Bianchi for the preparation and processing of the sequencing libraries; F. Cilenti for help with immunofluorescence experiments; I. Amit (Weizmann Institute) for the shRNA vectors targeting *Junb* and *Cebpb*; and D. Voehringer (University Hospital Erlangen, Germany for the *Stat6*−/− bone marrow cells. Supported by the European Research Council (Advanced ERC grant to G.N.), the Italian Ministry of University and Research (FIRB RBAP11H2R9 to G.N.), the Telethon Foundation (SR-Tiget Grant Award TGT16F04 to R.O.), the Cariplo Foundation (Giovani Ricercatori, 2015-0990 to R.O.) and the Italian Association for Research on Cancer (B.A.).

AUTHOR CONTRIBUTIONS

V.P., R.O. and G.N., conceptualization; V.P., analysis of all data and generation of figures; A.C. and R.O., design and carrying out of most experiments; M.G., S.G., M.S., generation of a subset of the data; A.S. and B.A., provision of critical reagents; R.O. and G.N., acquisition of funding; and G.N., supervision, and writing of the manuscript with input from all authors.

COMPETING FINANCIAL INTERESTS

The authors declare no competing financial interests.

1. Glass, C.K. & Natoli, G. Molecular control of activation and priming in macrophages. *Nat. Immunol.* **17**, 26–33 (2016).
2. Murray, P.J. *et al.* Macrophage activation and polarization: nomenclature and experimental guidelines. *Immunity* **41**, 14–20 (2014).
3. Sica, A. & Mantovani, A. Macrophage plasticity and polarization: in vivo veritas. *J. Clin. Invest.* **122**, 787–795 (2012).
4. Lawrence, T. & Natoli, G. Transcriptional regulation of macrophage polarization: enabling diversity with identity. *Nat. Rev. Immunol.* **11**, 750–761 (2011).
5. Gordon, S. & Martinez, F.O. Alternative activation of macrophages: mechanism and functions. *Immunity* **32**, 593–604 (2010).
6. Murray, P.J. & Wynn, T.A. Protective and pathogenic functions of macrophage subsets. *Nat. Rev. Immunol.* **11**, 723–737 (2011).
7. Ostuni, R. *et al.* Latent enhancers activated by stimulation in differentiated cells. *Cell* **152**, 157–171 (2013).
8. Monticelli, S. & Natoli, G. Short-term memory of danger signals and environmental stimuli in immune cells. *Nat. Immunol.* **14**, 777–784 (2013).
9. Netea, M.G. *et al.* Trained immunity: A program of innate immune memory in health and disease. *Science* **352**, aaf1098 (2016).
10. Lavin, Y. *et al.* Tissue-resident macrophage enhancer landscapes are shaped by the local microenvironment. *Cell* **159**, 1312–1326 (2014).
11. Xue, J. *et al.* Transcriptome-based network analysis reveals a spectrum model of human macrophage activation. *Immunity* **40**, 274–288 (2014).
12. Allen, J.E. & Maizels, R.M. Diversity and dialogue in immunity to helminths. *Nat. Rev. Immunol.* **11**, 375–388 (2011).
13. Elliott, D.E. & Weinstock, J.V. Helminth-host immunological interactions: prevention and control of immune-mediated diseases. *Ann. NY Acad. Sci.* **1247**, 83–96 (2012).
14. Osborne, L.C. *et al.* Virus-helminth coinfection reveals a microbiota-independent mechanism of immunomodulation. *Science* **345**, 578–582 (2014).

15. Reese, T.A. *et al.* Helminth infection reactivates latent γ-herpesvirus via cytokine competition at a viral promoter. *Science* **345**, 573–577 (2014).
16. Salgame, P., Yap, G.S. & Gause, W.C. Effect of helminth-induced immunity on infections with microbial pathogens. *Nat. Immunol.* **14**, 1118–1126 (2013).
17. Harris, J. *et al.* T helper 2 cytokines inhibit autophagic control of intracellular Mycobacterium tuberculosis. *Immunity* **27**, 505–517 (2007).
18. Potian, J.A. *et al.* Preexisting helminth infection induces inhibition of innate pulmonary anti-tuberculosis defense by engaging the IL-4 receptor pathway. *J. Exp. Med.* **208**, 1863–1874 (2011).
19. Schleicher, U. *et al.* TNF-mediated restriction of arginase 1 expression in myeloid cells triggers type 2 NO synthase activity at the site of infection. *Cell Rep.* **15**, 1062–1075 (2016).
20. Ostuni, R., Kratochvill, F., Murray, P.J. & Natoli, G. Macrophages and cancer: from mechanisms to therapeutic implications. *Trends Immunol.* **36**, 229–239 (2015).
21. Creyghton, M.P. *et al.* Histone H3K27ac separates active from poised enhancers and predicts developmental state. *Proc. Natl. Acad. Sci. USA* **107**, 21931–21936 (2010).
22. Rada-Iglesias, A. *et al.* A unique chromatin signature uncovers early developmental enhancers in humans. *Nature* **470**, 279–283 (2011).
23. Kaikkonen, M.U. *et al.* Remodeling of the enhancer landscape during macrophage activation is coupled to enhancer transcription. *Mol. Cell* **51**, 310–325 (2013).
24. Ivashkiv, L.B. & Donlin, L.T. Regulation of type I interferon responses. *Nat. Rev. Immunol.* **14**, 36–49 (2014).
25. Andersson, R. *et al.* An atlas of active enhancers across human cell types and tissues. *Nature* **507**, 455–461 (2014).
26. Pello, O.M. *et al.* Role of c-MYC in alternative activation of human macrophages and tumor-associated macrophage biology. *Blood* **119**, 411–421 (2012).
27. Kress, T.R., Sabo, A. & Amati, B. MYC: connecting selective transcriptional control to global RNA production. *Nat. Rev. Cancer* **15**, 593–607 (2015).
28. Jenkins, S.J. *et al.* Local macrophage proliferation, rather than recruitment from the blood, is a signature of TH2 inflammation. *Science* **332**, 1284–1288 (2011).
29. Sieweke, M.H. & Allen, J.E. Beyond stem cells: self-renewal of differentiated macrophages. *Science* **342**, 1242974 (2013).
30. Qiao, Y. *et al.* Synergistic activation of inflammatory cytokine genes by interferon-γ-induced chromatin remodeling and toll-like receptor signaling. *Immunity* **39**, 454–469 (2013).

ONLINE METHODS

Mice and cell cultures. Animal experiments were performed in accordance with the Italian Laws (D.L.vo 116/92), which enforce the EU 86/609 Directive. Bone-marrow-derived macrophage (BMDMs) were prepared *ex vivo* from mouse bone marrow cells cultured in L929-conditioned medium containing M-CSF as described[31]. After 6 d in culture, adherent cells were >99% $Cd11b^+$ $F4/80^+$, as assessed by flow cytometry. Infections were carried out as described[31]. *Junb* and *Cebpb* lentiviral shRNA vectors were gifts from I. Amit (Weizman Institute). BM cells from Stat6-deficient mice were a gift from D. Voehringer (University Hospital Erlangen, Germany).

Cytokines and antibodies. Recombinant mouse IFN-γ and IL-4 were from R&D Systems; unless otherwise stated, cytokines were used at a concentration of 100 ng/ml and 10 ng/ml, respectively. Anti-IL4 blocking antibody (clone 11B11) was from eBioscience and used at 1 μg/ml. Antibodies used in ChIP experiments, to STAT1 (sc-592), STAT6 (sc-981), MYC (sc-764), JUNB (sc-46x) and C/EBPβ (sc-150X), were all from Santa Cruz and used at 10 μg per ChIP. Anti-H3K27ac (ab4729) was from Abcam (2.5 μg per ChIP). The rabbit polyclonal antibody to PU.1 was generated in-house against the N terminus of PU.1 (amino acids 1–100; NP_035485.1)[32] and used at 5 μg per ChIP. Antibodies used for immunoblot analysis (1:1,000 dilution) were to the following: STAT1 (#9172), phospo-STAT1 (Tyr701, #9171), Stat6 (#9362), phospho-Stat6 (Tyr641, #9361), Erk1/2 (#9102), phospho-Erk1/2 (Thr202/Tyr204, #9101), phospho-Akt (Ser473, #9271), all from Cell Signaling; actin (Sigma-Aldrich, A4700); and vinculin (Santa Cruz, sc-5573). Antibodies to the following were used for flow cytometry: CD11b (clone M1/70, 1:500 dilution), F4/80 (BM8, 1:40 dilution) and Nos2 (CXNFT, 1:500 dilution), all from eBioscience; and phospho-STAT1-AlexaFluor 647 (Cat. 612597, 1:100 dilution) and phospho-STAT6-PE (Cat. 558252, 1:100 dilution), both from BD Biosciences. Antibodies to the following were used for immunofluorescence: phospho-STAT1-AlexaFluor 647 (Cat. 612597, 1:20 dilution) and phospho-STAT6-PE (Cat. 558252, 1:20 dilution) from BD Biosciences; DAPI (Cat. 62247, 100 μg/ml) was from Thermo Scientific.

Flow cytometry with intracellular staining. After cytokine stimulation for the time indicated in the figures, BMDMs were collected and stained with LYVEDEAD Fixable Yellow (L34959, Molecular Probes) for dead-cell exclusion and with anti-CD11B. For intracellular staining of iNOS, cell fixation and permeabilization were performed using buffers and protocols from eBiosciences (00-8222-49/56). For analyses of phospho-STAT1 and phospho-STAT6, cells were fixed with BD PhosflowTM Fix Buffer I (Cat. No. 557870) at 37 °C for 10 min, washed and permeabilized with BD PhosflowTM Perm Buffer III (Cat. No. 558050). Cells were resuspended in FACS buffer and analyzed on a FACSCanto II (BD Biosciences). The specificity of the staining was verified with isotype-matched control antibody (clone eBM2a from eBioscience, 1:500 dilution), unstained controls and fluorescence-minus-one (FMO) controls. Data were analyzed with FACS DIVA Software 6.1.2 (BD Biosciences) and FlowJo Software 9.3.2.

Immunofluorescence analysis. Bone marrow cells were plated on coverslips within a six-well plate at a density of 1×10^5 cells per well and differentiated for 6 d. BMDM were then stimulated with IFN-γ or IL-4 or both cytokines, washed with cold PBS and fixed with 1% paraformaldehyde (PFA) in PBS at room temperature (RT) for 10 min. Fixed cells were then permeabilized with cold methanol (100%) for 10 min at −20 °C, were washed three times with 0.3% Triton X-100 in PBS, and were blocked for 1 h with blocking buffer (5% BSA in 0.3% Triton-X100/PBS). For the analysis of phospho-STAT1 and phospho-STAT6, cells were stained with conjugated antibodies overnight at 4 °C. Cells were counterstained with DAPI for 10 min at RT, and were mounted with Aqua/Poly mount (Polysciences, Cat. 18606) on slides. Images were taken on a Nikon Eclipse E600 microscope (1024 × 1024, 40hex) or on a Leica TCS SP2 confocal microscope (1024 × 1024, 40hex, 2× optical zoom) and analyzed with Fiji ImageJ software (v 2.0.0-rc-43).

ChIP-seq. ChIP was carried out as previously described[7]. In brief, 1×10^6 to 3×10^6 macrophages (for H3K27ac ChIP-Seq) or 5×10^7 to 10×10^7 macrophages (for transcription factors) were fixed with 1% formaldehyde, and nuclear fractions isolated and lysed. After chromatin shearing by sonication, lysed nuclei were incubated overnight at 4 °C with protein G Dynabeads (Life Technologies) previously coupled with 2.5–10 μg of antibody. Beads were recovered using a 96-well magnet washed extensively, and DNA was eluted and decrosslinked overnight at 65 °C. DNA was purified with solid-phase reversible immobilization (SPRI) beads (Agencourt AMPure XP, Beckman Coulter) and was quantified with PicoGreen (Life Technologies). 1–5 ng of ChIP DNA was used for ChIP-Seq library preparation, using a previously described protocol[33] with minor modifications[7] and was sequenced on a HiSeq2000 (Illumina).

RNA analysis. Total RNA was isolated using RNeasy Mini Kit (Qiagen) with in-column DNase treatment, quantified with Nanodrop (ThermoScientific) and reverse transcribed using ImProm-II RT (Promega) according to the manufacturers' instructions. 10 ng of cDNA were used for amplification. mRNA-Seq library preparation from 1 μg of total RNA was performed with the TruSeq RNA Sample Prep kit (Illumina) and sequenced on a HiSeq2000 (Illumina).

Computational methods. Single-end reads (51 nt) were quality-filtered according to the Illumina pipeline and mapped to the mm10 reference genome. For ChIP-Seq, reads were mapped using Bowtie2 v 2.2.6 (ref. 34). We used default parameters with the options–very-sensitive,–no-unal and with the pre-built bowtie2 index. Only uniquely mapping reads were retained. Peak calling for acetylation was performed using SICER v1.1 (ref. 35) using a redundancy threshold of 1, a window size of 200 bp, a gap size of 600 bp and a false-discovery rate (FDR) cutoff of 1×10^{-3}. Fragment size was set to 150 and the effective genome fraction to 0.80. Peak calling for TFs was performed using MACS2 v.2.1.0.20150731 (ref. 36), using default parameters with the exception of the bandwidth (–bw 100), the minimum q-value cutoff for peaks detection (-q 0.01) and the effective genome size (-g 1.87e9). For RNA-Seq, single-reads were mapped using TopHat v2.1.0 using the option–b2-very-sensitive[37]. Differential expression was evaluated with an exact test for the negative binomially distributed counts using edgeR v3.10.5 with limma v3.24.15 Bioconductor package[38–41]. Detailed computational methods are described in the **Supplementary Note**.

Data availability. Raw data sets are available for download at the Gene Expression Omnibus (GEO) database (http://www.ncbi.nlm.nih.gov/gds/) under accession code GSE84520.

31. Austenaa, L.M. *et al.* Transcription of mammalian cis-regulatory elements is restrained by actively enforced early termination. *Mol. Cell* **60**, 460–474 (2015).
32. Mancino, A. *et al.* A dual cis-regulatory code links IRF8 to constitutive and inducible gene expression in macrophages. *Genes Dev.* **29**, 394–408 (2015).
33. Garber, M. *et al.* A high-throughput chromatin immunoprecipitation approach reveals principles of dynamic gene regulation in mammals. *Mol. Cell* **47**, 810–822 (2012).
34. Langmead, B. & Salzberg, S.L. Fast gapped-read alignment with Bowtie 2. *Nat. Methods* **9**, 357–359 (2012).
35. Zang, C. *et al.* A clustering approach for identification of enriched domains from histone modification ChIP-Seq data. *Bioinformatics* **25**, 1952–1958 (2009).
36. Zhang, Y. *et al.* Model-based analysis of ChIP-Seq (MACS). *Genome Biol.* **9**, R137 (2008).
37. Kim, D. *et al.* TopHat2: accurate alignment of transcriptomes in the presence of insertions, deletions and gene fusions. *Genome Biol.* **14**, R36 (2013).
38. Robinson, M.D., McCarthy, D.J. & Smyth, G.K. edgeR: a Bioconductor package for differential expression analysis of digital gene expression data. *Bioinformatics* **26**, 139–140 (2010).
39. Robinson, M.D. & Oshlack, A. A scaling normalization method for differential expression analysis of RNA-seq data. *Genome Biol.* **11**, R25 (2010).
40. Robinson, M.D. & Smyth, G.K. Small-sample estimation of negative binomial dispersion, with applications to SAGE data. *Biostatistics* **9**, 321–332 (2008).
41. McCarthy, D.J., Chen, Y. & Smyth, G.K. Differential expression analysis of multifactor RNA-Seq experiments with respect to biological variation. *Nucleic Acids Res.* **40**, 4288–4297 (2012).